

# Sliding wear: role of plasticity

R. Xu<sup>1,2,3</sup> and B.N.J. Persson<sup>1,2,3</sup>

<sup>1</sup>*Peter Grünberg Institute (PGI-1), Forschungszentrum Jülich, 52425, Jülich, Germany*

<sup>2</sup>*State Key Laboratory of Solid Lubrication, Lanzhou Institute of Chemical Physics, Chinese Academy of Sciences, 730000 Lanzhou, China*

<sup>3</sup>*MultiscaleConsulting, Wolfshovener str. 2, 52428 Jülich, Germany*

**Abstract:** We present experimental wear data for polymethyl methacrylate (PMMA) sliding on tile, sandpaper, and polished steel surfaces, as well as for silica glass and quartz sliding on sandpaper. The experimental results are compared with a recently developed theory of sliding wear[1]. Our findings demonstrate that wear on surfaces with roughness below a critical threshold cannot result from crack propagation induced by frictional shear stress in block-substrate asperity contact regions and must, therefore, originate from a different mechanism.

**Corresponding author:** B.N.J. Persson, email: b.persson@fz-juelich.de

## 1 Introduction

Wear is the progressive loss of material from a solid body due to its contact and relative movement against a surface [2–11]. Wear particles can have an adverse influence on the health of living organisms, or result in the breakdown of mechanical devices. There are several limiting wear processes, known as *fatigue wear*, *abrasive wear*, and *adhesive wear*.

*Fatigue wear* occurs when a polymer block slides on a rigid countersurface with “smooth roughness.” In this scenario, the stress concentrations in asperity contact regions are relatively low, requiring multiple contacts to remove polymer particles. This wear process involves fatigue failure rather than tensile failure, where material removal is gradual. The abrasion caused by this failure mode is known as fatigue wear.

*Abrasive wear*, in contrast, arises when a polymer block slides against surfaces with sharp asperities. High stress concentrations at the asperity tips cut into the polymer, potentially exceeding the material’s limiting strength, leading to micro-cutting or scratching. This results in longitudinal scratches, called score lines, parallel to the sliding direction. Abrasive wear is primarily driven by mechanical interactions between the harder surface asperities and the softer polymer, making it distinct from fatigue wear.

*Adhesive wear* involves the transfer of material between contacting surfaces due to adhesive forces. It frequently occurs when one block slides on another block made of the same material. For example, in metallic systems, “cold welded” junctions can form in the contact regions, and as these junctions break during sliding, the material is transferred from one surface to the other. Although less common in polymers, adhesive wear may still occur under specific conditions, such as decomposition of ma-

terials.

Many polymers have important medical applications, but sometimes polymer wear results in severe health or other problems. For example, high-density polyethylene (HDPE) or ultra-high-molecular-weight polyethylene (UHMWPE) has been used as a bearing component in total joint replacements. However, the wear of HDPE and UHMWPE when sliding on the counter surface generates small polymer particles, which can induce an inflammatory response in the surrounding tissue, leading to osteolysis, where bone tissue is resorbed [12]. Over time, this may result in implant loosening or failure. Similarly, polymethyl methacrylate (PMMA) is commonly used for prosthetic dental applications, including the fabrication of artificial teeth, where wear may limit the useful lifetime.

Understanding crack propagation is essential for analyzing polymer wear. The crack or tearing energy  $\gamma$  (defined as the energy per unit area required to separate surfaces at a crack tip) provides a key measure of material resistance to crack growth [13]. For polymers,  $\gamma$  can range from  $\sim 10^2$  to  $\sim 10^5$  J/m<sup>2</sup>, depending on factors such as crack tip velocity and temperature. This should be compared to the crack energy for (brittle) crystalline solids, which is on the order of  $\sim 1$  J/m<sup>2</sup>, even for solids with strong covalent bonds like diamonds. The large  $\gamma$  values in polymers arise from energy contributions due to chain stretching, uncrosslinked chain pull-out, and mechanisms like crazing, cavitation, and viscoelastic dissipation near the crack tip.

The crack energy  $\gamma$  has been extensively studied in cases of constant crack tip velocity [14] and oscillating strains [15–17], both yield similar results. Under oscillatory strain, the crack tip displacement  $\Delta x$  per strain cycle depends on  $\gamma$ . Below a lower critical value  $\gamma_0$  (e.g.,  $\sim 50$  J/m<sup>2</sup> for PMMA), no crack growth occurs, while  $\Delta x$  diverges as  $\gamma$  approaches the ultimate tear strength  $\gamma_1$  (e.g.,  $\sim 500$  J/m<sup>2</sup> for PMMA). However, unless  $\gamma$  is close to  $\gamma_1$ , the crack tip displacement  $\Delta x$  is very small.

Hence, several stress cycles may be needed to remove a particle from a PMMA surface under *fatigue wear*.

Crack energy measurements are typically conducted on macroscopic samples (samples with linear dimensions  $\sim 1$  cm), which may not represent the smaller length scales in polymer wear, where particles as small as  $\sim 1 \mu\text{m}$  are removed. At these scales, contributions from mechanisms such as cavitation and crazing may be reduced. Additionally, in sliding the asperity-induced deformation spans a broad frequency range ( $\omega \approx v/r_0$ , where  $v$  is the sliding speed and  $r_0$  is the contact size), unlike the fixed frequency conditions used in tearing energy experiments.

In Ref. [1], a theory was developed to describe sliding wear in rubber. In this study, we extend this theory to PMMA wear. Wear rates of PMMA sliding on tile, sandpaper, and polished steel surfaces under dry conditions are measured and compared with theoretical predictions.

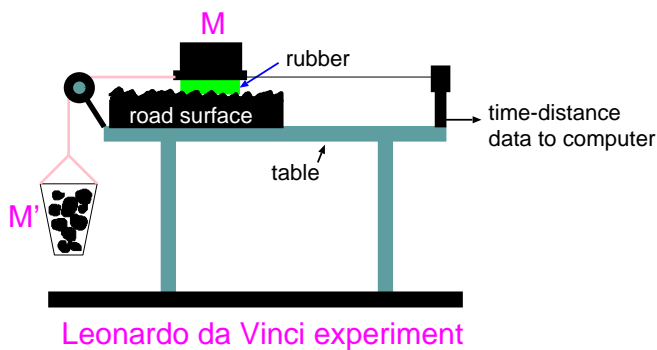


FIG. 1. A simple friction slider (schematic) measures the sliding distance  $x(t)$  via a displacement sensor.

## 2 Experimental methods

The data used in the present study were obtained using the setup shown in Fig. 1. The slider consists of two PMMA (or glass) blocks glued to a metal plate, with one block positioned at the front and the other at the back. The nominal contact area is  $A_0 \approx 20 \text{ cm}^2$ . The normal force  $F_N$  is determined by the total mass  $M$  of lead blocks placed on top of the metal plate. Similarly, the driving force is determined by the total mass of the lead blocks in the container,  $M'$ . Three different substrates are used: ceramic tile, sandpaper P100, and polished steel.

The sliding distance  $x(t)$  as a function of time  $t$  is measured using a displacement sensor. This simple friction slider setup can also be used to calculate the friction coefficient  $\mu = M'/M$  as a function of sliding velocity and nominal contact pressure  $p_0 = Mg/A_0$ . Note that with this setup, the driving force is specified, allowing the study of the velocity dependence of friction only on the branch of the  $\mu(v)$  curve where the friction coefficient increases with increasing speed. For PMMA sliding the

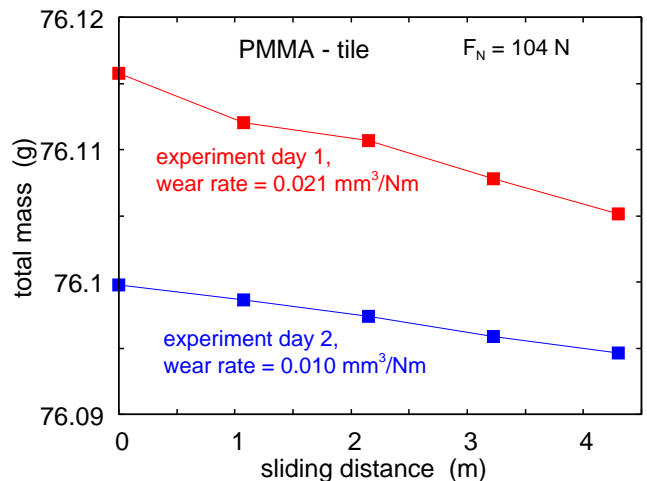


FIG. 2. The mass of the PMMA blocks and metal plate as a function of the sliding distance on the tile surface. Experiments performed on two consecutive days gave different results: on the first day, the wear rate was  $\Delta V/F_N L = 0.021 \text{ mm}^3/\text{Nm}$ , while on the second day it was  $0.01 \text{ mm}^3/\text{Nm}$ . The wear volume was calculated from the wear mass using the PMMA mass density  $\rho = 1180 \text{ kg/m}^3$ . In the experiments, the normal load was  $F_N = 104 \text{ N}$ , with a nominal contact area of  $A_0 = 20 \text{ cm}^2$ , resulting in a nominal contact pressure of  $\sigma = 0.052 \text{ MPa}$ .

studied surfaces, the friction coefficient is very weakly velocity-dependent. Sometimes unstable sliding occurs, resulting in a sliding speed that fluctuates over time. The average sliding speed in our studies was  $\sim 3 \text{ mm/s}$ .

To study the velocity and pressure dependence of the wear rate, we slid the metal plate with the PMMA blocks on the studied surfaces. Each sliding act consisted a distance of 21.5 cm on tile, 18 cm on sand paper, and 10 cm on polished steel. The wear rate was determined from the mass change (the difference in the mass of the PMMA blocks before and after sliding) using a high-precision balance (Mettler Toledo analytical balance, model MS104TS/00) with a sensitivity of 0.1 mg. Between each sliding act, we clean the surface using a brush or a single-use nonwoven fabric.

The surface roughness of all surfaces used in this study was measured using a Mitutoyo Portable Surface Roughness Measurement SurfTest SJ-410. The instrument is equipped with a diamond tip with a radius of curvature of  $R = 1 \mu\text{m}$  and operates with a tip-substrate repulsive force of  $F_N = 0.75 \text{ mN}$ . Measurements were taken with a step length (pixel) of  $0.5 \mu\text{m}$ , a scan length of  $L = 25 \text{ mm}$ , and a tip speed of  $v = 50 \mu\text{m/s}$ .

## 3 Experimental results

We have measured the wear rate and the friction force of PMMA and glass blocks which was slid on studied

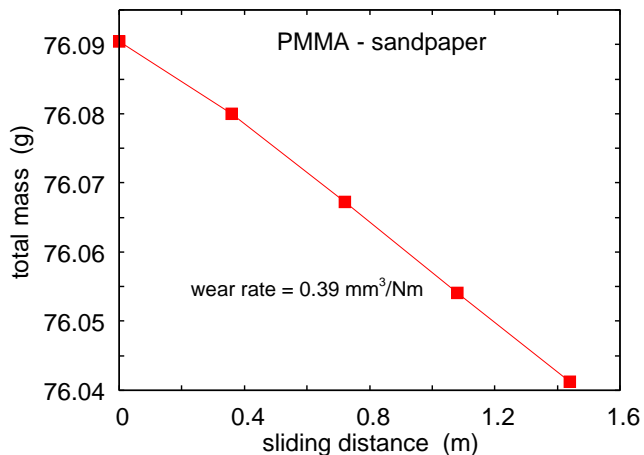


FIG. 3. The mass of the PMMA blocks and metal plate as a function of the sliding distance on the tile surface. Experiments performed on two consecutive days gave different results: on the first day, the wear rate was  $\Delta V/F_N L = 0.021 \text{ mm}^3/\text{Nm}$ , while on the second day it was  $0.01 \text{ mm}^3/\text{Nm}$ . The wear volume was calculated from the wear mass using the PMMA mass density  $\rho = 1180 \text{ kg/m}^3$ . In the experiments, the normal load was  $F_N = 104 \text{ N}$ , with a nominal contact area of  $A_0 = 20 \text{ cm}^2$ , resulting in a nominal contact pressure of  $\sigma = 0.052 \text{ MPa}$ .

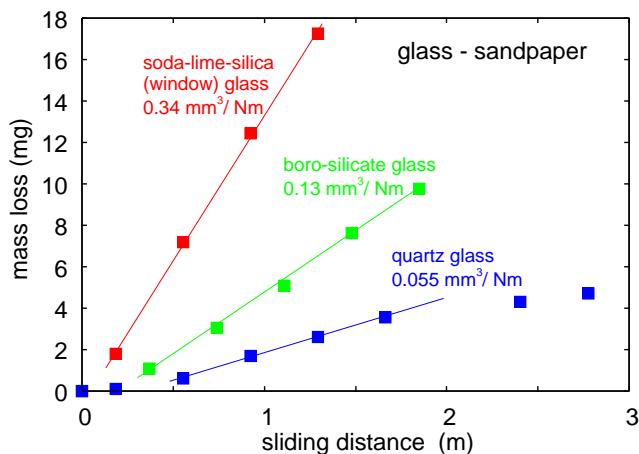


FIG. 4. The mass loss of blocks made of soda-lime glass (red), borosilicate glass (green), and quartz glass as a function of the sliding distance. The substrate used is sandpaper P100. The wear rates,  $\Delta V/F_N L$ , are indicated in the figure. In the experiments, the normal load was  $F_N = 104 \text{ N}$ , with a nominal contact area of  $A_0 = 20 \text{ cm}^2$ , resulting in a nominal contact pressure of  $\sigma = 0.052 \text{ MPa}$ .

surfaces. In all experiments, the normal load was  $F_N = 104 \text{ N}$ , and the nominal contact area was  $A_0 = 20 \text{ cm}^2$ , giving a nominal contact pressure of  $p_0 = 0.052 \text{ MPa}$ . Since PMMA, ceramic tile, sandpaper, and polished steel are elastically relatively stiff, the PMMA blocks do not contact the substrate surfaces uniformly at the macroscopic level. This non-uniform contact is evident from the distribution of the wear tracks on the PMMA surface

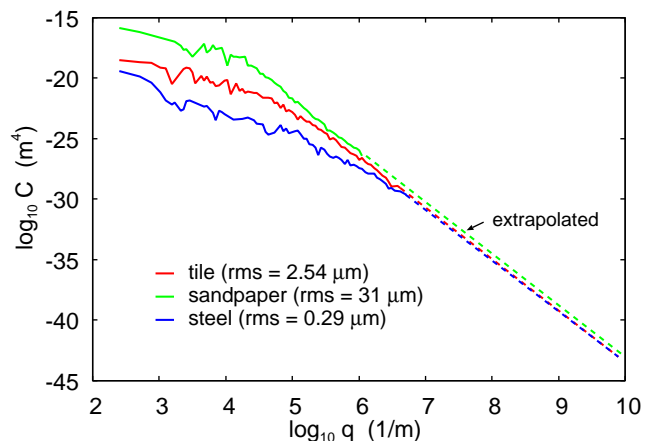


FIG. 5. The surface roughness power spectra of the tile, steel and sandpaper surfaces used in the wear studies. The dotted regions are extrapolated with a slope corresponding to the Hurst exponent  $H \approx 1$ .

after a sliding act. Consequently, the nominal contact pressure is not uniform but varies on the length scale of the size of the PMMA blocks.

Fig. 2 shows the mass of the PMMA blocks and metal plate as a function of the sliding distance for the tile surface. Experiments performed on two consecutive days gave different results: on the first day, the wear rate was  $\Delta V/F_N L = 0.021 \text{ mm}^3/\text{Nm}$ , while on the second day, it was  $0.010 \text{ mm}^3/\text{Nm}$ . Here, we calculated the wear volume from the mass loss, assuming a PMMA mass density of  $\rho = 1180 \text{ kg/m}^3$ . In both measurements, the wear rate was proportional to the sliding distance, suggesting that the difference in wear rate between the two days must be due to changes in external conditions (e.g., humidity, which was not measured) or some aging process that altered the properties of the worn PMMA or tile surface. We did not observe any PMMA particles adhering to the tile surface, but we cannot exclude the possibility that the tile surface asperities were covered by a nanometer-thin film of PMMA.

For PMMA on the sandpaper P100 surface, a significantly higher wear rate was observed, with  $\Delta V/F_N L = 0.39 \text{ mm}^3/\text{Nm}$ . In contrast, for the polished steel surface, no mass change was detected after a sliding distance of 4 m. However, given that the resolution of the measuring instrument was 0.1 mg, it is possible that a smaller amount of wear may have occurred but was below the detection limit.

The wear produced a white powder of PMMA particles, which was easily brushed away after each sliding act. The PMMA wear particles were much smaller than the rubber wear particles observed in an earlier experiment, and we were unable to study the size of the PMMA wear particles using the same optical microscope used to study rubber

wear particles in Ref. [1].

The wear rate for glass blocks sliding on the sandpaper P100 surface is shown in Fig. 4. The figure presents the mass loss of blocks made of soda-lime glass (red), borosilicate glass (green), and quartz glass as a function of the sliding distance. The wear rates,  $\Delta V/F_N L = 0.34, 0.13,$  and  $0.055 \text{ mm}^3/\text{Nm}$  for the three glass types, respectively, are indicated in the figure.

Fig. 5 shows the surface roughness power spectra of the tile, sandpaper, and steel surfaces used in the wear studies. The dotted regions represent extrapolated sections with a slope corresponding to the Hurst exponent  $H \approx 1$ . Both the tile and steel surfaces are harder and elastically stiffer than PMMA, so these materials are treated as rigid, with no deformation of their surface roughness profiles. The sandpaper surface is composed of very hard corundum (aluminum oxide) particles, which can be considered rigid, when in contact with PMMA and even with the glass surfaces. (Note: the penetration hardness of corundum is  $\sim 30 \text{ GPa}$ , compared to  $\sim 15 \text{ GPa}$  for quartz.) However, the corundum particles are embedded in a polymer fiber mat containing an acrylic resin (see Fig. 6), which is elastically and plastically much softer than silica glass and has properties likely similar to PMMA. When sandpaper contacts silica glass surfaces, the surface roughness components with wavelengths longer than the size of the corundum particles (diameter  $D \approx 160 \mu\text{m}$  for P100 sandpaper; see Fig. 6) are easily flattened. These components should not be included in the wear rate calculations for the silica glass surfaces if the substrate is treated as rigid. For this reason, we exclude the roughness components with wavenumbers  $q < 2\pi/D \approx 4 \times 10^4 \text{ m}^{-1}$  from the power spectrum of the sandpaper surface (green line in Fig. 5) when calculating wear rates for silica glass surfaces.

For PMMA on sandpaper, it is less clear whether this same power spectrum correction is necessary. However, for consistency, we apply the same long-wavelength cut-off for PMMA as for the silica surfaces in the present study.

#### 4 Theory of sliding wear

Sliding wear depends on the size of contact regions and on the stress acting in the contact regions[18]. In Ref. [1], we have developed a theory of sliding wear. Here, we present an alternative derivation of the main result.

Cracks at the surface of a solid can be induced by both the normal and the tangential stress acting on the surface, but particle removal is caused mainly by the tangential stress. Let  $\tau = \tau(\zeta_r)$  be the effective shear stress acting in an asperity contact region with a radius  $r_0$ . The magnification  $\zeta_r$  is determined by the radius of the contact region,  $q_r = \pi/r_0$ ,  $\zeta_r = q_r/q_0$ . The elastic energy

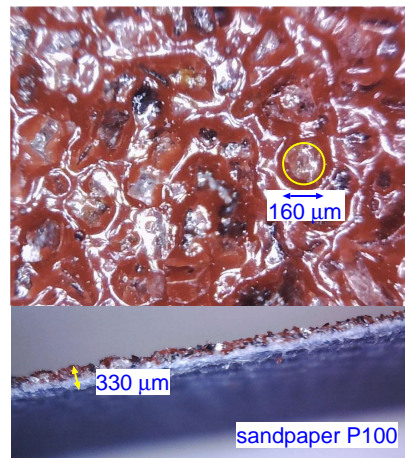


FIG. 6. Top: Picture of sandpaper P100. The corundum particles have an average diameter of  $\approx 160 \mu\text{m}$ . Bottom: Cross-section of the sandpaper. The sandpaper P100 has a thickness of  $\approx 330 \mu\text{m}$ .

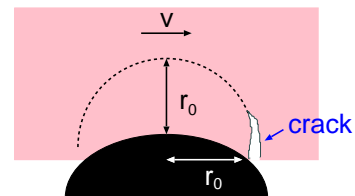


FIG. 7. A PMMA block sliding in contact with a hard counter-surface. The sliding speed  $v$  and the radius of the contact region  $r_0$  are indicated. The deformation field extends into the polymer a similar distance as it extends laterally.

stored in the deformed asperity contact is (see Fig. 7)

$$U_{\text{el}} \approx \frac{\tau^2}{E^*} r_0^3,$$

where the effective modulus  $E^* = E/(1-\nu^2)$  (we assume that the substrate is rigid). More accurately, assume that the shear stress acts uniformly within a circular region with a radius  $r_0$ . The center of the circular region will displace a distance  $u$  given by  $ku = F$ , where  $F = \tau\pi r_0^2$  is the force and  $k \approx (\pi/2)E^*r_0$  the spring constant. This gives the elastic energy

$$U_{\text{el}} = \frac{1}{2}ku^2 = \frac{F^2}{2k} = \frac{(\pi r_0^2 \tau)^2}{\pi E^* r_0} = \pi \frac{\tau^2}{E^*} r_0^3. \quad (1)$$

In order for the shear stress to remove a particle of linear size  $r_0$ , the stored elastic energy must be larger than the fracture (crack) energy, which is of the order

$$U_{\text{cr}} \approx \gamma 2\pi r_0^2, \quad (2)$$

where  $\gamma$  is the energy per unit surface area to break the bonds at the crack tip. If  $U_{\text{el}} > U_{\text{cr}}$ , the elastic energy is large enough to propagate a crack and remove

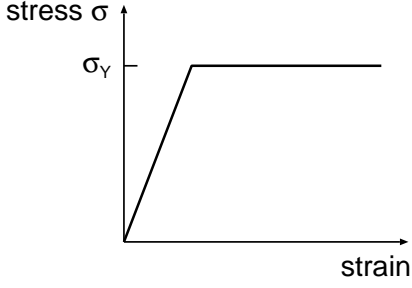


FIG. 8. The relation between the stress and the strain in elongation for the simplest elastoplastic model assumes that the maximum stress equals the yield stress,  $\sigma_Y$ . The penetration hardness is typically  $\sigma_P \approx 3\sigma_Y$ , where  $\sigma_P$  represents the ratio between the indentation force and the indentation cross-sectional area.

a particle[4–6]. Thus, for a particle to be removed, we must have  $\tau > \tau_c$ , where

$$\tau_c = \beta \left( \frac{2E^* \gamma}{r_0} \right)^{1/2}, \quad (3)$$

where  $\beta$  is a number of order unity, which takes into account that the wear particles, in general, are not hemispherical as assumed above.

In what follows, we will treat the polymer surface as smooth and assume only roughness on the counter surface. We will denote a substrate asperity, where the shear stress is high enough to remove a particle of size  $r_0$ , as a *wear-asperity*, and the corresponding contact region as the *wear-contact region*.

If we assume that during sliding, the effective shear stress  $\tau$  is proportional to the normal stress  $\sigma$ ,  $\tau = \mu\sigma$ , we find that particles will be removed only if the contact stress  $\sigma > \sigma_c(\zeta)$ , where

$$\sigma_c = \frac{\beta}{\mu} \left( \frac{2E^* \gamma}{r_0} \right)^{1/2}. \quad (4)$$

For randomly rough surfaces, for elastic contact the probability distribution of contact stress equals:

$$P(\sigma, \zeta) = \frac{1}{(4\pi G)^{1/2}} \left( e^{-(\sigma-\sigma_0)^2/4G} - e^{-(\sigma+\sigma_0)^2/4G} \right), \quad (5)$$

where  $\sigma_0$  is the nominal (applied) pressure and where

$$G = \frac{\pi}{4} (E^*)^2 \int_{q_0}^{\zeta q_0} dq q^3 C(q), \quad (6)$$

where  $C(q)$  is the surface roughness power spectrum.

When the stress in the asperity contact region becomes high enough, plastic flow occurs. In the simplest model, it is assumed that a material deforms as a linear elastic solid until the stress reaches a critical level, the so-called

plastic yield stress, where it flows without strain hardening (see Fig. 8). The yield stress in elongation is denoted by  $\sigma_Y$ . In indentation experiments, where a sharp tip or a sphere is pushed against a flat solid surface, the penetration hardness  $\sigma_P$  is defined as the ratio between the normal force and the projected (on the surface plane) area of the plastically deformed indentation. Typically,  $\sigma_P \approx 3\sigma_Y$ .

The influence of plastic flow on the contact mechanics can be taken into account in the Persson contact mechanics approach by replacing the boundary condition  $P(\infty, \zeta) = 0$  with the condition that there is no stress at the interface above the penetration hardness, i.e.,  $P(\sigma, \zeta) = 0$  for  $\sigma > \sigma_P$ . Thus, the maximum stress at the interface is equal to the penetration hardness  $\sigma_P$ . This approach is based on the simplest elastoplastic description, where only elastic deformation occurs for  $\sigma < \sigma_P$ , while for  $\sigma = \sigma_P$ , the material flows without work-hardening so that the maximal stress equals  $\sigma_P$  (see Fig. 8). The pressure probability distribution for this case is given by[19]:

$$P(\sigma, \zeta) = \frac{2}{\sigma_P} \sum_{n=1}^{\infty} \sin(s_n \sigma_0) \sin(s_n \sigma) e^{-s_n^2 G(\zeta)} + P_{pl}(\zeta) \delta(\sigma - \sigma_P) \quad (7)$$

where  $s_n = n\pi/\sigma_P$  and

$$P_{pl} = \frac{\sigma_0}{\sigma_P} + \frac{2}{\pi} \sum_{n=1}^{\infty} \frac{(-1)^n}{n} \sin(s_n \sigma_0) e^{-s_n^2 G(\zeta)} \quad (8)$$

As  $\sigma_P \rightarrow \infty$ , (7) reduces to (5). The  $P(\sigma, \zeta)$  is also the pressure distribution resulting from *elastic* deformations if the two surfaces are separated and brought into contact again at the same position. Hence, it is the pressure distribution that should be used to obtain the elastic energy, which enters into the theory of the wear rate.

In Fig. 9, we show  $P(\sigma, \zeta)$  as a function of the stress  $\sigma$  for  $\zeta = 1857$  for PMMA in contact with the tile surface, with the power spectrum given by the red curve in Fig. 5. The tile surface is considered as rigid and the PMMA elastic (green curve) or elastoplastic (red curve) with the penetration hardness  $\sigma_P = 0.4$  GPa.

When the interface is studied at the magnification  $\zeta$ , the area  $A = A_{wear}(\zeta)$ , where the shear stress is high enough to remove particles, is given by

$$\frac{A_{wear}(\zeta)}{A_0} = \int_{\sigma_c(\zeta)}^{\infty} d\sigma P(\sigma, \zeta). \quad (9)$$

When we study the interface at the magnification  $\zeta$ , the smallest wear particles observed have the size  $r_0 \approx \pi/q_r$ , with  $q_r = \zeta q_0$ . We may say that at the magnification

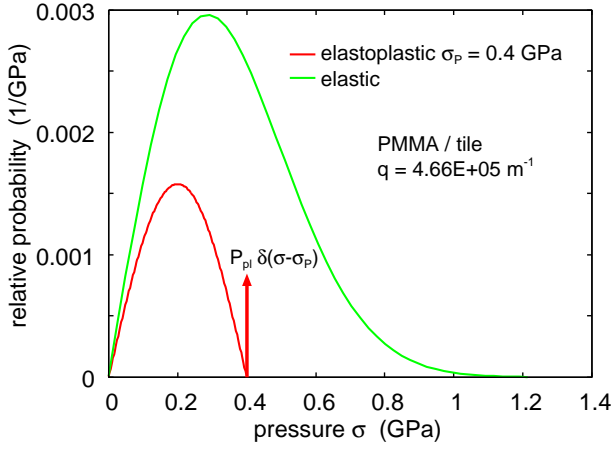


FIG. 9. The stress probability distribution  $P(\sigma, \zeta)$  as a function of the stress  $\sigma$  for PMMA in contact with the tile surface, with the power spectrum given by the red curve in Fig. 5. The magnification  $\zeta = q/q_0$ , with  $q = 4.66 \times 10^5 \text{ m}^{-1}$  and  $q_0 = 251 \text{ m}^{-1}$ . The tile surface is considered as rigid and the PMMA as elastic (green curve) with  $E = 3 \text{ GPa}$  and  $\nu = 0.3$ , or elastoplastic (red curve) with  $\sigma_P = 0.4 \text{ GPa}$ .

$\zeta$ , there is a pixel size of  $r_0 = \pi/\zeta q_0$ , and the smallest removed particle, which can be observed at this magnification, is determined by the pixel size. As previously stated, such a particle can be removed from the polymer surface if  $U_{el} > U_{cr}$ , where  $U_{el}$  is the stored elastic energy ( $\sim r_0^3$ ) in a volume element of linear size  $r_0$ , and  $U_{cr}$  is the energy needed to break the bonds and detach the particle.  $U_{cr} \approx \gamma 2\pi r_0^2$ , where  $\gamma$  is the energy per unit surface area to propagate the crack. The crack energy  $\gamma$  depends on the speed of bond-breaking and will take a range of values,  $\gamma_0 < \gamma < \gamma_1$ . The faster the crack propagates, the larger  $\gamma$  becomes. The smallest stored elastic energy  $U_{el} = U_{el0}$ , which can remove a particle, is given by  $U_{el0} \approx \gamma_0 2\pi r_0^2$ , but for this case, the crack moves extremely slowly, and the incremental displacement  $\Delta x$  during the interaction between the (moving) *wear-asperity* and the crack is very small, requiring many  $\sim r_0/\Delta x$  contacts to remove the particle. If the interaction with a *wear-asperity* results in  $U_{el} \gg U_{el0}$ , the crack will move much faster ( $\Delta x$  is much bigger), and far fewer contacts are needed to remove a particle. During sliding, the crack will be in contact with many *wear-asperities* of different sizes, so it will experience a wide range of crack-tip movements  $\Delta x$  before the particle is finally removed.

The probability that the stress at an arbitrary point on the polymer surface is between  $\sigma$  and  $\sigma + d\sigma$ , when the interface is studied at the magnification  $\zeta$ , is given by  $P(\sigma, \zeta)d\sigma$ . If  $\sigma > \sigma_c$ , the local stress results in  $U_{el} > U_{el0}$ , so in principle, a particle could be removed. But during the interaction time, the crack moves only the distance  $\Delta x(\gamma)$ , where we assume the relevant  $\gamma$  is given by  $U_{el} = \gamma r_0^2$ . Hence,  $N(\gamma) = r_0/\Delta x$  contacts are needed to remove

the particles. Thus, after the run-in, the probability that a particle will be removed from the regions where the stress is in the range  $\sigma$  to  $\sigma + d\sigma$  will be  $P(\sigma, \zeta)d\sigma/N(\gamma)$ . The total probability will be

$$P^* = \int_{\sigma_c}^{\infty} d\sigma \frac{P(\sigma, \zeta)}{1 + r_0(\zeta)/\Delta x(\sigma, \zeta)} \quad (10)$$

where we have added 1 in the denominator in order for the limit  $\Delta x/r_0 \rightarrow \infty$  to be correct. In (10), the cut-off stress  $\sigma_0$  is determined by  $U_{el} = U_{el0}$ . There are  $N^* = A_0/\pi r_0^2$  pixels on the surface, so sliding the distance  $L = 2r_0$  will result in removing  $N^*P^*$  particles, corresponding to the volume  $V = (2\pi r_0^3/3)N^*P^*$ . Thus, we get  $V/L = (\pi r_0^2/3)N^*P^*$  or  $V/LA_0 = P^*/3$ . Using (10), this gives

$$\frac{V}{LA_0} = \frac{1}{3} \int_{\sigma_c}^{\infty} d\sigma \frac{P(\sigma, \zeta)}{1 + r_0(\zeta)/\Delta x(\sigma, \zeta)} \quad (11)$$

which is the same as (17) in Ref. [1], except that the factor of 1/2 in (17) in Ref. [1] is replaced by 1/3 in (10) due to a slightly different description of the particle removal process. Eq. (11) shows that the wear volume per unit sliding length is proportional to the nominal surface area, as expected when the nominal contact pressure is constant.

The number of contacts needed to remove a particle  $N_{cont} \approx r_0/\Delta x$  depends on the crack energy  $\gamma$ , but it could be a large number ( $10^2$  or more) if the macroscopic relation between the tear-energy  $\gamma$  and  $\Delta x$  would also hold at the length scale of the wear particles.

The theory above gives the wear volume assuming that particles of a given size (radius  $r_0$ ) are generated. These are the (smallest) particles observed at the magnification  $\zeta = q_r/q_0 = \pi/q_0 r_0$ . To get the total wear volume, we need to sum up the volume of the wear particles from all length scales, which can be observed as we increase the magnification. In order not to count particles of similar size twice, we will increase the magnification in steps of factors of  $\sim 2$  and write  $\zeta = 2^n = \zeta_n$ , where  $n = 0, 1, \dots, n_1$  and  $2^{n_1} q_0 = q_1$ . We will refer to the interval from  $\zeta = 2^n$  to  $2^{n+1}$  as a 2-interval. Using

$$\sum_{n=0}^{n_1} f_n \approx \int_0^{n_1} dn f_n = \frac{1}{\ln 2} \int_1^{\zeta_1} d\zeta \frac{1}{\zeta} f(\zeta),$$

we can write the total wear volume when  $\Delta x$  is constant as

$$\begin{aligned} \frac{V}{A_0 L} &\approx \frac{1}{3} \sum_{n=0}^{n_1} \frac{1}{1 + r_0(\zeta_n)/\Delta x} \frac{A_{wear}(\zeta_n)}{A_0} \\ &\approx \frac{1}{3 \ln 2} \int_1^{\zeta_1} d\zeta \frac{1}{\zeta} \frac{1}{1 + r_0(\zeta)/\Delta x} \frac{A_{wear}(\zeta)}{A_0}. \end{aligned} \quad (12)$$

Using  $\zeta r_0 = \pi/q_0$ , this gives

$$\frac{V}{A_0 L} \approx \frac{1}{3 \ln 2} \int_1^{\zeta_1} d\zeta \frac{1}{\zeta + \pi/q_0 \Delta x} \frac{A_{wear}(\zeta)}{A_0}$$

$$= \frac{1}{3\ln 2} \int_{q_0}^{q_1} dq \frac{1}{q + \pi/\Delta x} \frac{A_{\text{wear}}(q)}{A_0}. \quad (13)$$

When  $\Delta x$  depends on  $\gamma$ , we get

$$\frac{V}{A_0 L} = \frac{1}{3\ln 2} \int_{q_0}^{q_1} dq \int_{\sigma_c(\zeta)}^{\infty} d\sigma \frac{P(\sigma, \zeta)}{q + \pi/\Delta x(\sigma, \zeta)}, \quad (14)$$

where  $\zeta = q/q_0$ . It is convenient to write  $q = q_0 e^\xi$ , so that  $dq = q d\xi$ , and

$$\frac{V}{A_0 L} = \frac{1}{3\ln 2} \int_0^{\xi_1} d\xi \int_{\sigma_c(\zeta)}^{\infty} d\sigma \frac{P(\sigma, \zeta)}{1 + r_0(\zeta)/\Delta x(\sigma, \zeta)}. \quad (15)$$

where  $\xi_1 = \ln(q_1/q_0)$ .

If we write

$$Q(\sigma, \zeta) = \frac{P(\sigma, \zeta)}{1 + r_0(\zeta)/\Delta x(\sigma, \zeta)}$$

we can define the average number of contacts needed to remove a particle of size  $r_0 = \pi/\zeta q_0$  as

$$\langle N_{\text{cont}} \rangle = \frac{\int_{\sigma_c(\zeta)}^{\infty} d\sigma N_{\text{cont}}(\sigma, \zeta) Q(\sigma, \zeta)}{\int_{\sigma_c(\zeta)}^{\infty} d\sigma Q(\sigma, \zeta)} \quad (16)$$

where

$$N_{\text{cont}}(\sigma, \zeta) = 1 + r_0(\zeta)/\Delta x(\sigma, \zeta).$$

The distribution of particles of different sizes is given by (17) [or (18)]. Thus, the number of particles with radius  $r_0$  between  $(\pi/q_0)2^{-n-1/2}$  and  $(\pi/q_0)2^{-n+1/2}$  is

$$\frac{N_n}{A_0 L} \approx \frac{1}{3\pi r_0^3(\zeta_n)[1 + r_0(\zeta_n)/\Delta x]} \frac{A_{\text{wear}}(\zeta_n)}{A_0} \quad (17)$$

or, when  $\Delta x$  depends on  $\gamma$ ,

$$\frac{N_n}{A_0 L} \approx \frac{1}{3\pi r_0^3(\zeta_n)} \int_{\sigma_c(\zeta_n)}^{\infty} d\sigma \frac{P(\sigma, \zeta_n)}{1 + r_0(\zeta_n)/\Delta x(\sigma, \zeta_n)}. \quad (18)$$

The theory presented above assumes that all length scales contribute independently to the wear rate. This cannot be strictly true since a long crack, which would result in a large wear particle, will change the stress field in its vicinity out to a distance of the order of the length of the crack. This effect, known as crack shielding, reduces the ability for smaller cracks to grow in the neighborhood of longer cracks. However, crack tip shielding is much weaker for sliding contacts as compared to polymer strips elongated by uniform far-field stress.

Note that if  $r_0/\Delta x$  is large, a long run-in distance would be needed before the wear reaches a steady state. This is particularly true if the nominal contact pressure is small, where the distance between the wear asperity contact regions may be large. However, since the contact regions

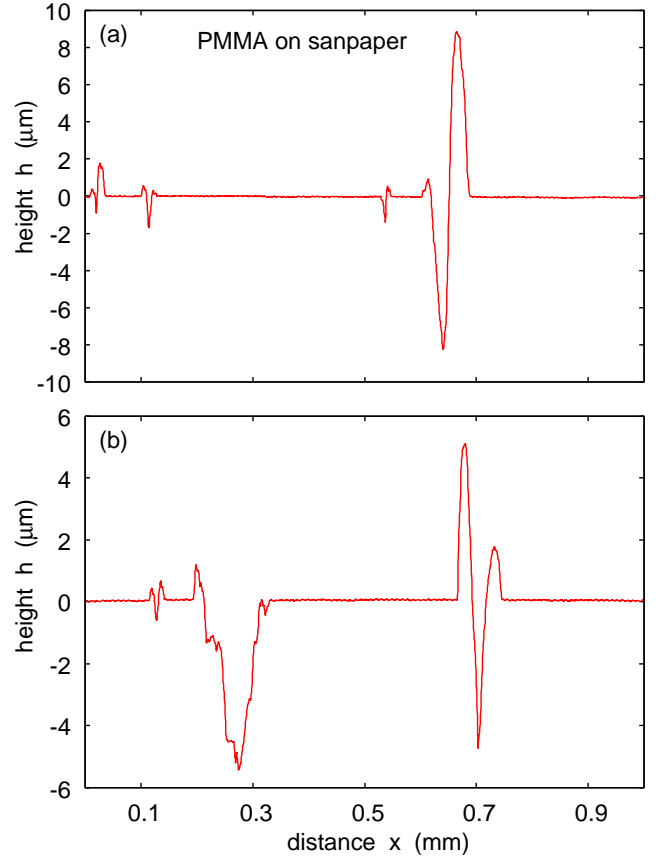


FIG. 10. The height profile orthogonal to the ploughing tracks after a PMMA block was slid a short distance on a sandpaper P100 surface. Note that most of the PMMA removed from the ploughing tracks does not form wear particles but is plastically displaced on the surface. An analysis of a 10 mm long wear track shows less than  $\sim 10\%$  of the material in the wear tracks is removed as wear particles.

within the macroasperity contacts are densely distributed and independent of the nominal contact pressure, there may, in some cases, be enough wear asperity contact regions within the macroasperity contact regions to reach the  $N_{\text{cont}}$  needed for wear particle formation even over a short sliding distance.

## 5 Role of plastic flow

In the context of sliding wear, asperity contact regions may deform plastically at short length scales even if brittle fracture occurs at long length scales. This has been observed even for very brittle materials such as silicon nitride. The reason why plastic flow rather than crack propagation may occur at short length scales can be understood based on the Griffith fracture criterion[4–6, 20?]: To remove a particle of linear size  $r_0$ , the local stress must be so large that the stored elastic energy in a volume element  $\sim r_0^3$  is larger than the fracture energy  $\sim \gamma r_0^2$ . This gives the condition  $\sigma > \sigma_c$ , where  $\sigma_c$  is given by (4),

for the removal of a particle. If  $\sigma_c$  is larger than the penetration hardness  $\sigma_P$  on the length scale  $r_0$ , no crack propagation can occur, and the material will flow plastically at this length scale. This fact is utilized in *ductile mode cutting*, where materials are removed from a surface by plastic flow instead of brittle fracture, resulting in a less damaged surface[21, 22]. Thus, when a hard (e.g., diamond) asperity is slid on the surface of a brittle solid at low enough load (where the linear size of the contact is small enough), it can remove material by cutting (producing micro or nano chips) without creating cracks at the surface. This method is used to machine surfaces of brittle solids like silica glass, silicon, silicon nitride, or tungsten carbide[21, 22]. (Cutting occurs when material is separated from the surface in the form of primary debris, or microchips, with little or no material displaced to the sides of the grooves. This mechanism closely resembles conventional machining.)

In many cases, plastic flow will not remove material from a surface but just displace it[10, 11]. Thus, if the asperity slopes are not too high, we expect the formation of ploughing tracks, where material is displaced to the neighborhood of the tracks rather than removed as (free) wear particles, as expected for sharper roughness. The amount of displaced material can be deduced from line topography measurements performed on a very flat surface of the material under study. If sliding over a surface area occurs only once at low contact pressure, the separation between the ploughing tracks will be large. We denote the flat surface regions between the ploughing tracks as the *undeformed surface plane*. The volume of material removed as particles can be deduced from the difference in the volume of material below and above the undeformed surface plane. To illustrate this, in Fig. 10, we show a short segment of a 10 mm long line scan for PMMA that was slid a short distance on a sandpaper surface. In this case, by analyzing the ploughing tracks from the whole line scan, we find that more than  $\sim 90\%$  of the volume of material removed below the undeformed surface plane is displaced rather than removed as wear particles. The same was observed on silica glass surfaces (see Appendix A).

In the study below, we will use the Persson contact mechanics theory to take into account plastic deformation. This is expected to be a reasonable approach as long as the plastic deformations are small but may fail if deep ploughing wear tracks occur. The basic picture behind this approach is as follows:

When a block is squeezed against a substrate with a force  $F_N$  that results in plastic flow, a new (modified) surface profile forms once the external force is removed. If the external force is applied again, the solids will deform elastically up to the same force  $F_N$  as applied in the first step. This implies that the elastic energy  $U_{el}$  stored in the as-

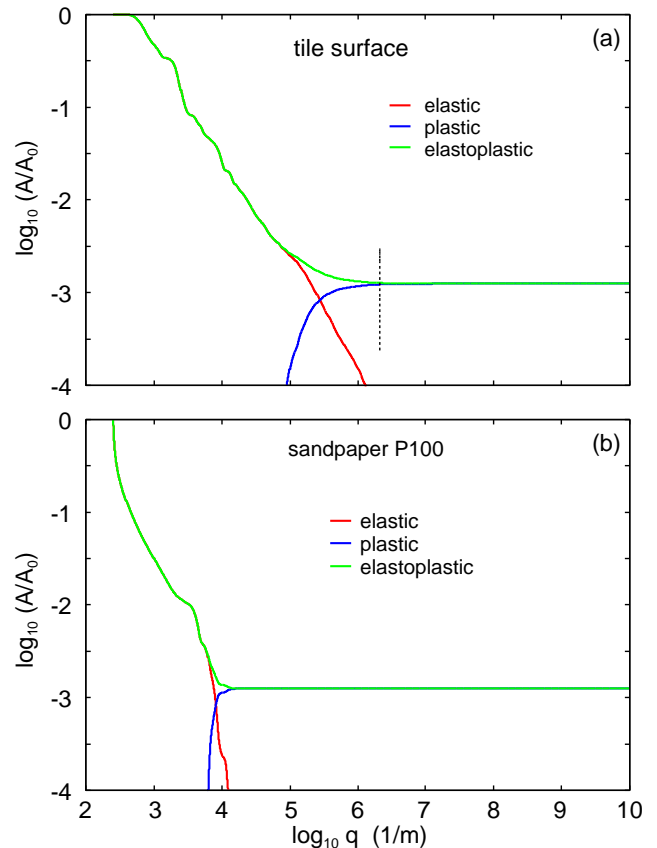


FIG. 11. The area of real contact as a function of the largest wavenumber  $q$  included in the calculation, for PMMA on the tile surface (a) and on the sandpaper P100 surface (b). The wavenumber  $q$  is related to the magnification  $\zeta$  via  $q = \zeta q_0$ . The red and blue lines are elastic and plastic contact areas, and the green line is the elastic contact area for the elastoplastic deformed surface. We have assumed elastoplastic contact with the Young's modulus  $E = 3$  GPa, the Poisson ratio  $\nu = 0.3$ , and the penetration hardness  $\sigma_P = 0.4$  GPa.

perity contact regions can be calculated from the stress probability distribution (7).

Some plastic flow occurs in asperity contacts for PMMA in contact with all three substrate surfaces used in our study. However, for the steel surface, plastic flow only occurs at the nanoscale, which has no influence on the elastic energy stored in the wear asperity contact region, which involves length scales  $\sim 0.1 - 100 \mu\text{m}$ . However, for the tile and sandpaper surfaces, plastic flow occurs at much larger length scales.

In Fig. 11(a), we show the area of real contact as a function of the cut-off wavenumber  $q$  for PMMA on the tile surfaces. Here, the cut-off wavenumber  $q$  is the wavenumber of the shortest wavelength roughness used in the calculation, related to the magnification  $\zeta$  via  $q = \zeta q_0$ . In the calculations, we have used the PMMA penetration hardness  $\sigma_P = 0.4$  GPa and assumed the sandpaper to be rigid.



When calculating the contact area for the wavenumber  $q = \zeta q_0$ , we only include the long-wavelength roughness with wavenumbers  $q_0 < q < q_0 \zeta$ . Note that all contact regions have yielded plastically when  $q \approx 2 \times 10^6 \text{ m}^{-1}$ , corresponding to a wavelength of order  $\sim 1 \text{ }\mu\text{m}$ .

The sandpaper P100 surface has a larger surface roughness power spectrum than the tile surface, and for PMMA in contact with the sandpaper surface, plastic deformation starts at longer length scales, as illustrated in Fig. 11(b). Thus, for this surface, plastic yielding starts already for  $q \approx 10^4 \text{ m}^{-1}$ , corresponding to a wavelength of order  $\sim 0.3 \text{ mm}$ , which is of the order of the average size of the sand particles.

## 6 Comparing theory with experiments

Here we compare the theoretical predictions for the wear rate with the experimental results for PMMA sliding on tile, sandpaper, and steel surfaces, as well as for silica glass sliding on the sandpaper surface.

### PMMA on Tile, Sandpaper, and Steel

We model PMMA as an elastoplastic material with a Young's modulus  $E = 3 \text{ GPa}$  and a Poisson ratio  $\nu = 0.3$ . The penetration hardness of PMMA depends on the indentation time, as it is a stress-augmented, thermally activated flow process. In this study, the indentation time is of the order  $\tau = r/v$ , where  $v$  is the sliding speed, and  $r$  is a characteristic length scale, approximately equal to the typical radius of a wear particle,  $r \approx 3 \text{ }\mu\text{m}$ . With a sliding speed of  $v \approx 3 \text{ mm/s}$ , the indentation time is estimated to be  $\tau \approx 10^{-3} \text{ s}$ .

For PMMA, the measured penetration hardness as a function of the strain rate is well described by the following relation (in MPa) (see Ref. [23]):

$$\sigma_P \approx 0.313 + 0.0325 \log_{10}(\tau_0/\tau), \quad (20)$$

where  $\tau_0 = 1 \text{ s}$ .

Using  $\tau \approx 10^{-3} \text{ s}$ , the penetration hardness is calculated as  $\sigma_P \approx 0.41 \text{ GPa}$ .

The tile and steel surfaces have much larger elastic modulus and penetration hardness than PMMA and are treated as rigid materials. The sandpaper consists of very hard and elastically stiff corundum (aluminum oxide) particles deposited on an elastically soft polymer film. As discussed in Sec. 3, we account for this by including only the substrate roughness components with wavenumber  $q > 2\pi/D$ , where  $D$  is the average diameter of the corundum particles. For the steel and tile surfaces, we use the top surface roughness power spectra shown in Fig. 5. For the sandpaper, we exclude the region  $q < 2\pi/D$ . In all cases, the measured power spectra are linearly extrapolated to larger wavenumbers on a log-log

scale. The slope of the extrapolated region corresponds to a Hurst exponent  $H \approx 1$ , but the exact form of this extrapolation is not critical for the wear rate calculations presented below.

Using the Persson contact mechanics theory for elastoplastic contact [Eq. (7)], Fig. 11 shows the contact area between a PMMA block and (a) the tile surface and (b) the sandpaper surface as a function of the magnification  $\zeta$ , or the wavenumber  $q = \zeta q_0$  of the largest roughness component included in the calculation. The steel surface is relatively smooth, and for this case, plastic deformation occurs only at very short length scales involving surface roughness components with wavelengths below  $\sim 100 \text{ nm}$ . These roughness components are not significant for the wear process studied here. Hence, for the steel surface, we treat the PMMA as perfectly elastic.

To calculate the wear rate, we need to know the relationship between  $\Delta x$  and  $\gamma$ . This relationship has been studied for PMMA and varies slightly depending on the type of PMMA used[24]. The measured relationship is well approximated as follows:

$$\Delta x = 0, \quad \text{for } \gamma < \gamma_0,$$

and

$$\Delta x = a \left( \sqrt{\gamma} - \sqrt{\gamma_0} \right)^2 \left( \frac{\sqrt{\gamma} - \sqrt{\gamma_0}}{\sqrt{\gamma_1} - \sqrt{\gamma}} \right)^{\sqrt{(\gamma_0/\gamma_1)}} \quad (21)$$

for  $\gamma_0 < \gamma < \gamma_1$ , where  $\gamma_0 = 36.0 \text{ J/m}^2$ ,  $\gamma_1 = 517.0 \text{ J/m}^2$ , and  $a = 5.3 \times 10^{-9} \text{ m}^3/\text{J}$ .

Note that  $\Delta x \rightarrow \infty$  as  $\gamma$  approaches  $\gamma_1$ .

Using the power spectra shown in Fig. 5 and the relation between  $\Delta x$  and  $\gamma$  given by (21), we present in Fig. 12(a) the cumulative wear volume and in Fig. 12(b) the number of generated particles as functions of the logarithm of the particle radius for the PMMA-tile system. The green lines represent the results obtained without considering plastic deformation using (5), with the power spectrum indicated by the red line in Fig. 11. The red and blue lines correspond to calculations including plasticity using (7).

The calculated wear rate for  $\sigma_P = 0.4 \text{ GPa}$  [blue line in Fig. 12(a)] is  $\Delta V/LF_N \approx 0.0085 \text{ mm}^3/\text{Nm}$ , which is consistent with the experimental values (0.021 and 0.010 from two separate measurements; see Sec. 3). The peak in the number of generated particles in Fig. 12(b) occurs at particle sizes approximately one order of magnitude smaller than in previous studies of rubber wear. This observation qualitatively agrees with optical images of the wear particles, although the resolution of the optical instruments used was insufficient to accurately measure the sizes of PMMA particles. The exact number of generated particles for different size ranges can be determined

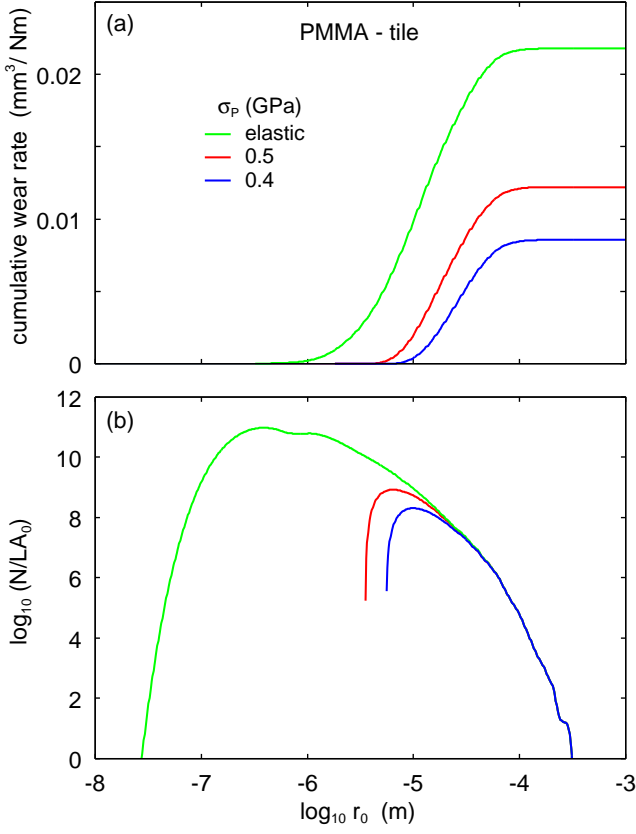


FIG. 12. (a) The cumulative wear volume and (b) the number of generated particles as functions of the logarithm of the particle radius for PMMA sliding on a tile surface. The wear rates without plastic deformation and with plastic deformation (assuming  $\sigma_P = 0.4$  GPa, blue line) are  $\approx 0.22 \text{ mm}^3/\text{Nm}$  and  $\approx 0.085 \text{ mm}^3/\text{Nm}$ , respectively. The measured wear rate is  $\approx 0.1 - 0.2 \text{ mm}^3/\text{Nm}$ . Calculations use  $E = 3$  GPa,  $\nu = 0.3$ , and the measured relation between the crack-tip displacement  $\Delta x(\gamma)$  and the tearing energy  $\gamma$ , shown in Fig. 13(a). The friction coefficient is  $\mu = 0.5$ , the nominal contact area  $A_0 = 0.002 \text{ m}^2$ , and the nominal contact pressure  $\sigma_0 = 0.052 \text{ MPa}$ , as in the experiment described in Sec. 3.

from Fig. 12(b) using the 2-interval separation method described in Ref. [1].

The relationship between  $\gamma$  and  $\Delta x$  depends on the specific PMMA type but generally follows the form given by (21), which is also depicted in Fig. 13(a). Note that  $\Delta x$  diverges as  $\gamma$  approaches the critical value  $\gamma_1$ . In Fig. 13(b), we display the integrand of (15) for PMMA on the tile surface as a function of  $\gamma$  for all magnifications (or particle radii  $r_0$ ), assuming no plastic flow (green lines) and including plasticity (red lines). While the integration variable in (15) is the pressure, each pressure value corresponds to tearing energy as defined by (4). The red and green areas represent the superposition of many curves corresponding to various magnifications or particle radii.

Fig. 14(a) shows the cumulative wear volume and (b)

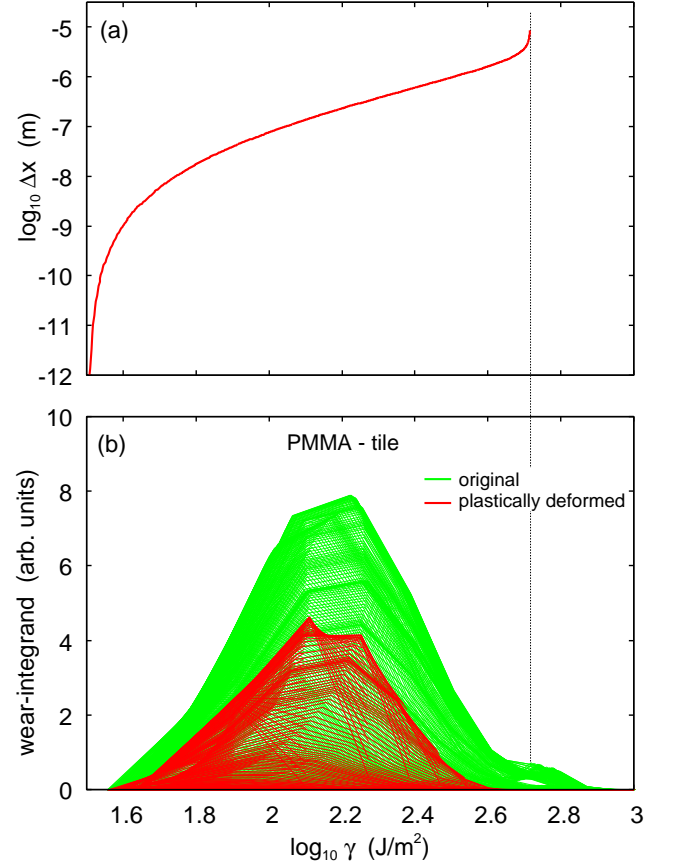


FIG. 13. (a) The relationship for PMMA between the crack tip displacement per oscillation and the tearing (or crack) energy  $\gamma$  based on the measurements presented in Ref. [? ]. (b) The integrand in (15) as a function of  $\gamma$  for all magnifications (or particle radius  $r_0$ ) for PMMA, for elastic contact (no plasticity) (green lines) and for elastoplastic contact with  $\sigma_P = 0.4$  GPa (red lines). We have used  $E = 3$  GPa,  $\nu = 0.3$ , and the relationship between the crack-tip displacement  $\Delta x(\gamma)$  and the tearing energy  $\gamma$  shown in (a). The nominal contact area  $A_0 = 0.002 \text{ m}^2$  and the nominal contact pressure  $\sigma_0 = 0.052 \text{ MPa}$ , as in the experiment described in Sec. 3. The friction coefficient  $\mu = 0.5$  was used in these calculations.

the number of generated particles as functions of the logarithm of the particle radius for PMMA-sandpaper. We have used the power spectrum of the sandpaper surface for  $q > 2\pi/D$  and the measured friction coefficient  $\mu = 0.60$ . The green line is calculated using (5) without plasticity, and the red lines include plastic flow using (7). The wear rate without and with plastic deformation (with  $\sigma_P = 0.4$  GPa) are  $\approx 1.74 \text{ mm}^3/\text{Nm}$  and  $0.40 \text{ mm}^3/\text{Nm}$ , respectively, while the measured wear rate is  $\approx 0.39 \text{ mm}^3/\text{Nm}$  (see Fig. 3).

For PMMA on the tile surface, several hundred contacts with wear asperities are needed to remove a single PMMA wear particle. This is illustrated in Fig. 15(a), where the green line shows the effective number of contacts  $\langle N_{\text{cont}} \rangle$

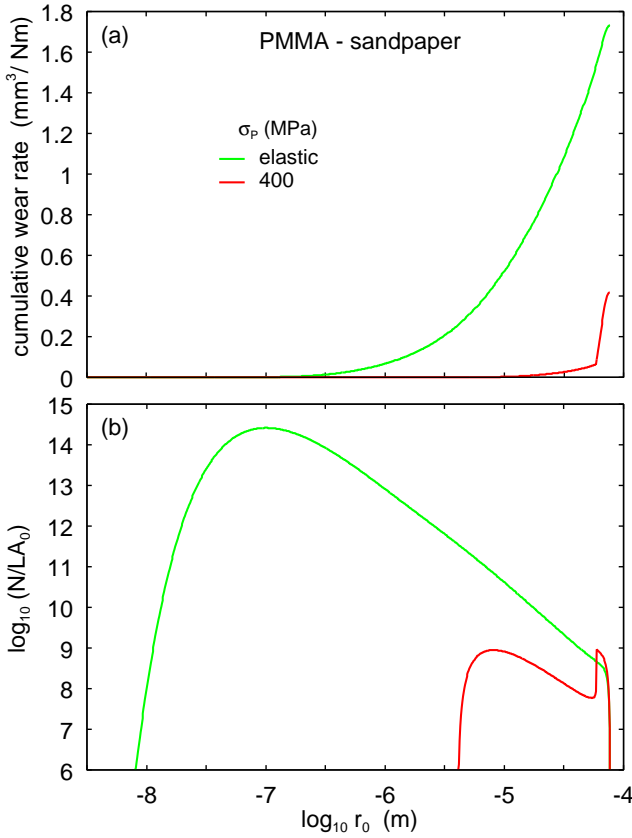


FIG. 14. (a) The cumulative wear volume, and (b) the number of generated particles, as a function of the logarithm of the particle radius for PMMA on sandpaper P100. The wear rate without and with plastic deformation (using  $\sigma_P = 0.4$  GPa) are approximately  $1.74 \text{ mm}^3/\text{Nm}$  and  $0.40 \text{ mm}^3/\text{Nm}$ , respectively. The measured wear rate is  $\approx 0.39 \text{ mm}^3/\text{Nm}$  (see Fig. 3). We have used  $E = 3$  GPa,  $\nu = 0.3$ , and the measured relationship between the crack-tip displacement  $\Delta x(\gamma)$  and the tearing energy  $\gamma$  shown in Fig. 13(a). The friction coefficient  $\mu = 0.6$ , the nominal contact area  $A_0 = 0.002 \text{ m}^2$ , and the nominal contact pressure  $\sigma_0 = 0.052 \text{ MPa}$  were the same as in the experiment described in Sec. 3.

needed to remove a wear particle, as a function of the logarithm of the wear particle radius. The red line in the figure, as also shown in Fig. 12(a), represents the cumulative wear volume, including plastic deformations, as a function of the logarithm of the wear particle radius. Approximately 70% of the wear mass is attributed to particles removed in fewer than  $\sim 500$  contacts with wear asperities.

For PMMA on the sandpaper surface, most wear particles are removed in a single contact between the PMMA and the corundum wear asperities. This is demonstrated in Fig. 15(b), where the sharp increase in the cumulative wear rate occurs when  $\langle N_{\text{cont}} \rangle \approx 0$ , corresponding to  $\Delta x \gg r_0$ .

Using the same parameters as above but with  $\mu =$

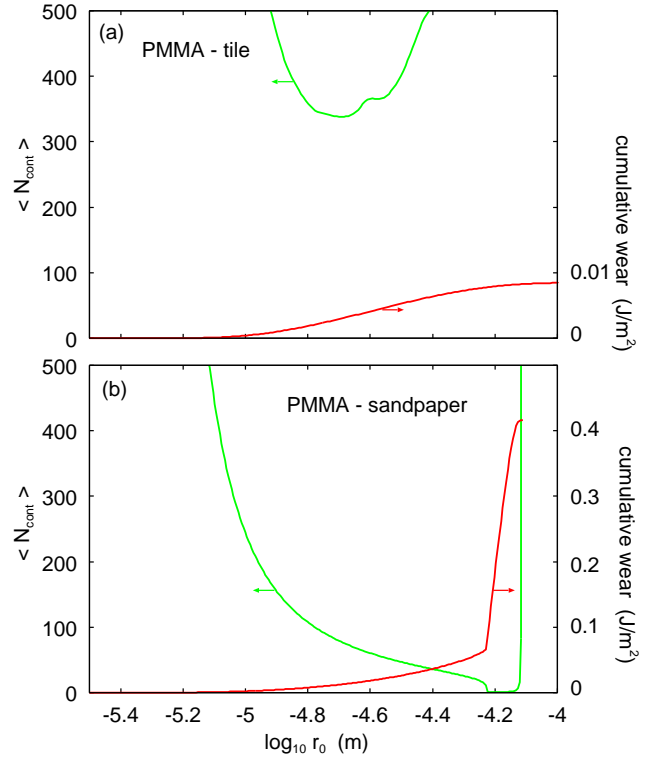


FIG. 15. The cumulative wear volume (red line) and the effective number of contacts ( $N_{\text{cont}}$ ) is required to remove a wear particle (green line) as a function of the logarithm of the wear particle radius. Results are shown for elastoplastic contact (with  $\sigma_P = 0.4$  GPa) for PMMA on (a) the tile surface and (b) the sandpaper surface. The nominal contact area is  $A_0 = 0.002 \text{ m}^2$  and the nominal contact pressure  $\sigma_0 = 0.052 \text{ MPa}$ , as in the experiment described in Sec. 3. The calculations use Young's modulus  $E = 3$  GPa, Poisson's ratio  $\nu = 0.3$ , and a friction coefficient  $\mu = 0.5$  for the tile surface and  $\mu = 0.6$  for the sandpaper surface.

0.2, for PMMA on the polished steel surface, with the power spectrum shown in Fig. 5 (blue line), we predict  $\Delta V/LF_N \approx 10^{-21} \text{ mm}^3/\text{Nm}$ , indicating negligible contribution to the wear resulting from the considered wear mechanism. This is consistent with our experiments, where no wear was detected after sliding 4 m on the steel surface. Given the resolution of our balance, which is 0.1 mg, this provides an upper limit of  $\sim 10^{-4} \text{ mm}^3/\text{Nm}$  for the wear rate.

### Silica glass and quartz on sandpaper

In Sec. 3, we studied the sliding wear for window (soda-lime-silica) glass, borosilicate glass, and quartz (crystalline  $\text{SiO}_2$ ) on sandpaper. The sandpaper consists of corundum (crystalline  $\text{Al}_2\text{O}_3$ ) particles, which are elastically stiffer and plastically harder than the glass, and we treat the sand particles as rigid. For silica glass and quartz, the Young's modulus is  $E \approx 70$  GPa, whereas for corundum,  $E \approx 350$  GPa. The penetration hard-

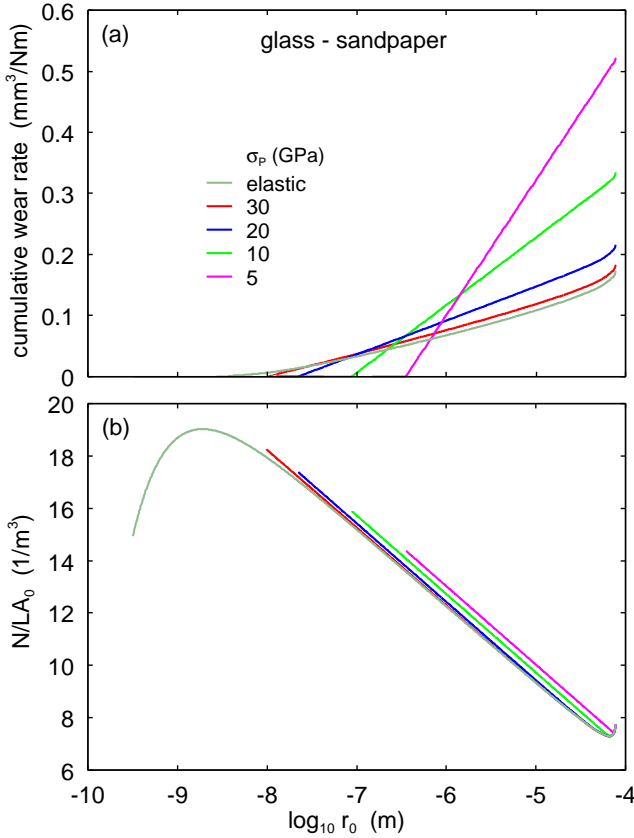


FIG. 16. The cumulative wear volume (a) and the number of wear particles (b) as a function of the logarithm of the wear particle radius for glass on sandpaper P100. Results are shown for different penetration hardness where the curve denoted “elastic” correspond to infinite hardness (no plastic flow). The nominal contact area  $A_0 = 0.002 \text{ m}^2$  and the nominal contact pressure  $\sigma_0 = 0.052 \text{ MPa}$ , as in the experiment described in Sec. 3. For the Young’s modulus  $E = 70 \text{ GPa}$ , Poisson ratio  $\nu = 0.3$  and the friction coefficient  $\mu = 0.34$ .

ness of corundum,  $\sigma_P \approx 22 \text{ GPa}$ , is higher than that of quartz,  $\sigma_P \approx 12 \text{ GPa}$  (from Ref. [25]), borosilicate glass,  $\sigma_P \approx 8 \text{ GPa}$  (from Ref. [26]), and soda-lime-silica glass,  $\sigma_P \approx 6 - 11 \text{ GPa}$  (from Ref. [27]), depending on the loading rate.

Fig. 16(a) shows the calculated cumulative wear rate and (b) the number of wear particles as a function of the logarithm of the wear particle radius for glass with different penetration hardness on sandpaper P100. The curve denoted “elastic” corresponds to infinite hardness (no plastic flow). The calculated wear rate for  $\sigma_P = 10 \text{ GPa}$  is  $\Delta V/LF_N \approx 0.33 \text{ mm}^3/\text{Nm}$ , which is similar to the measured wear rate for window glass ( $0.34 \text{ mm}^3/\text{Nm}$ ; see Fig. 4). However, the calculations cannot explain why the wear rates for borosilicate glass and quartz are approximately 0.38 and 0.16 times smaller, respectively, than for window glass (see Fig. 4).

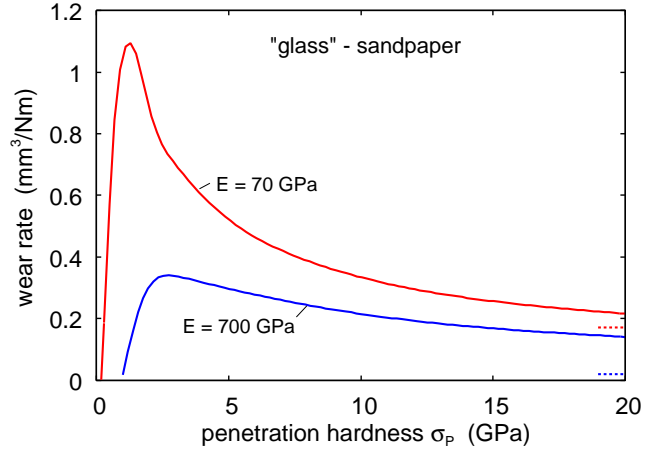


FIG. 17. The wear rate  $\Delta V/F_N L$  (in  $\text{mm}^3/\text{Nm}$ ) as a function of the penetration hardness for “glass” on the sandpaper P100 surface. The red and blue curves are for Young’s modulus  $E = 70 \text{ GPa}$  and  $E = 700 \text{ GPa}$ , respectively, and  $\nu = 0.3$ ,  $\mu = 0.34$ . The dotted red and blue lines are the wear rate assuming elastic contact ( $\sigma_P = \infty$ ).

## 7 Discussion

Many wear equations have been developed, but the most widely used is probably the Archard wear equation:

$$\frac{\Delta V}{LA_0} = K \frac{p_0}{\sigma_P} \quad (22)$$

where  $p_0$  is the (assumed constant) nominal contact pressure and  $A_0$  the nominal contact area, related to the applied normal force via  $F_N = p_0 A_0$ . We can also write (22) as

$$\frac{\Delta V}{F_N L} = \frac{K}{\sigma_P} \quad (23)$$

The parameter  $K$  is dimensionless but depends on the system under study and has been found to take a wide range of values. Eq. (23) assumes that all contact regions, when observed at the highest (atomic) resolution, have yielded plastically, and that the wear is related to removing fragments of material from the area of real contact. However, this equation (with  $K > 0$ ) cannot hold in general since, if  $U_{el} < U_{cr}$  on all length scales, no wear particles will form even though the contact regions may deform plastically. Furthermore, even if wear occurs, Eq. (22) is generally not valid, even if all contact regions have yielded plastically. We illustrate this in Fig. 17 for a hypothetical glass-sandpaper system.

Fig. 17 shows the calculated wear rate  $\Delta V/F_N L$  (in  $\text{mm}^3/\text{Nm}$ ) as a function of the penetration hardness for “glass” on the sandpaper P100 surface. The red and blue curves are for Young’s modulus  $E = 70 \text{ GPa}$  and  $E = 700 \text{ GPa}$ , respectively, with  $\nu = 0.3$  and  $\mu = 0.34$ . The dotted red and blue lines represent the wear rate assuming elastic contact ( $\sigma_P = \infty$ ). Note that for  $\sigma_P > 2.5 \text{ GPa}$ ,

in both cases, the wear rate decreases with increasing  $\sigma_P$  but slower than the  $1/\sigma_P$  predicted by Eq. (22). Furthermore, for small (but non-zero)  $\sigma_P$ , the wear rate vanishes. This is straightforward to understand since, for small enough  $\sigma_P$ , the stress at the interface is everywhere too small to generate wear particles, i.e.,  $U_{el} < U_{cr}$  for all length scales considered.

In the study above, we found that for PMMA on the tile surface,  $N_{cont} \gg 1$ . However, it is not clear if, during the relatively short sliding distances, points on the PMMA surface make contact with wear asperities as many times as expected from the large value of  $N_{cont}$ . This indicates that the relation  $\Delta x(\gamma)$  may need to be understood in a probabilistic framework, as we now discuss.

The Paris equation gives the crack-tip displacement  $\Delta x$  as a function of the tearing energy  $\gamma$  when a crack is exposed to an oscillating strain (or stress), e.g., from forces acting on the external boundary of the solid. When  $\gamma$  is close to the fatigue limit  $\gamma_0$ , very many oscillation periods are needed for the crack-tip displacement to become large enough to be measurable. It is usually assumed that cracks propagate continuously with the number of stress cycles, but here we propose a different scenario: We assume that crack propagation, when  $\gamma < \gamma_1$ , involves stress-aided thermally activated bond-breaking events, where segments at the crack tip move in irregularly distributed (in time) discrete steps, each of which may be much larger than an atomic distance. Hence, if  $U_{el} > U_{cr}$ , the factor  $1/(1 + r_0/\Delta x)$  may represent the probability of forming a wear particle in a single contact (of pixel size  $\sim r_0$ ) rather than the inverse of the number of contacts needed to form a wear particle. For example, if  $\Delta x = 10^{-11}$  m (or less) per cycle, which is expected if  $\gamma$  is sufficiently close to the fatigue limit  $\gamma_0$ , then during most stress cycles, no significant propagation occurs. However, occasionally, a segment along the crack line may displace by a characteristic distance that may be larger than an atomic distance.

The wear process described above arises from the elastic energy temporarily stored in asperity contact regions during sliding. If this elastic energy on a certain length scale  $r_0$  exceeds the critical value ( $U_{el} > U_{cr}$ ), crack propagation can result in the removal of particles or fragments of size  $r_0$  from the surfaces of the sliding solid bodies. However, if the roughness is small enough such that  $U_{el} < U_{cr}$  on all length scales in all asperity contact regions, wear of this type cannot occur. This phenomenon was illustrated with PMMA sliding on a steel surface, where  $\Delta V/LF_N \approx 10^{-21}$  mm<sup>3</sup>/Nm, while for the tile surface, with approximately 10 times higher rms roughness ( $\approx 3$   $\mu$ m instead of 0.3  $\mu$ m for the steel surface),  $\Delta V/LF_N \approx 0.01$  mm<sup>3</sup>/Nm. In general, there will be an abrupt transition with decreasing roughness from a regime of relatively high wear rates to one where the

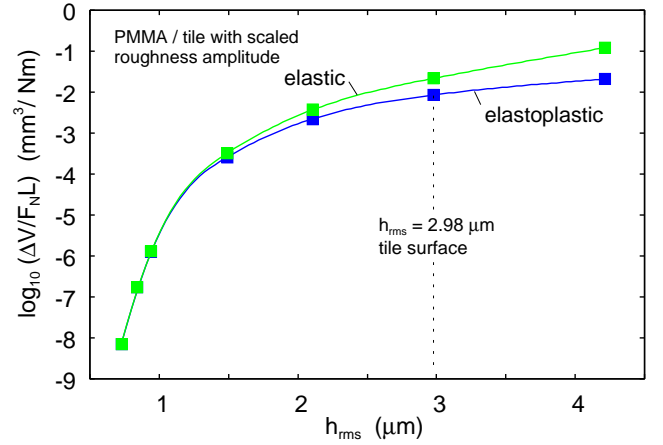


FIG. 18. The logarithm of the wear rate as a function of the rms roughness  $h_{rms}$  for PMMA in contact with a tile surface where the roughness is scaled so as to obtain surfaces with different roughness amplitude but the same fractal properties. The blue line is for elastoplastic contact with  $\sigma_P = 0.4$  GPa and the green line for elastic contact (no plasticity).

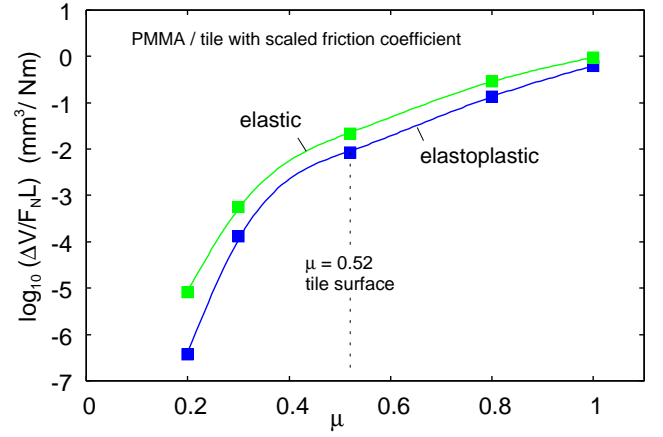


FIG. 19. The logarithm of the wear rate as a function of the friction coefficient for PMMA in contact with a tile surface where the friction coefficient is changed from the measured value 0.52 to smaller and larger values. The blue line is for elastoplastic contact with  $\sigma_P = 0.4$  GPa and the green line for elastic contact (no plasticity).

wear rate is extremely low. This is illustrated in Fig. 18, where the logarithm of the wear rate is shown as a function of the rms roughness, obtained by scaling the power spectrum of the tile surface. Note that for smooth surfaces (small  $h_{rms}$ ) no plastic flow occur and the elastoplastic result (blue line) gives the same result as with no plastic flow (green line). In a similar way, reducing the friction coefficient will reduce  $U_{el}$  and calculations show that for the PMMA / tile system if  $\mu$  is below  $\sim 0.15$  the wear rate vanish (see Fig. 19).

Many studies have been conducted on UHMWPE sliding on very smooth counter surfaces, as these systems

are of significant interest for artificial joints. The generation of wear debris has been recognized as one of the major causes of failure in total joint replacements. In most total joint replacements, one of the bearing surfaces consists of a hard, very smooth metal or ceramic material, while the other surface is made of UHMWPE. Wear particles generated from UHMWPE during sliding are released into the surrounding tissues, causing adverse cellular reactions that can lead to bone resorption and loosening. Thus, reducing the volume and number of UHMWPE wear particles is critical to improving the long-term clinical performance of total artificial joints.

In most artificial joint applications, the counter surface to the UHMWPE is extremely smooth, with an rms roughness below  $0.03 \mu\text{m}$ . For such surfaces, the wear mechanism described earlier cannot occur, and the observed wear rate is typically very low, on the order of  $10^{-8} \text{ mm}^3/\text{Nm}$ . The most likely origin of this wear is *polymer asperity wear*. The polymer surfaces in artificial joints often exhibit surface roughness with amplitudes of several micrometers (rms roughness of approximately  $1 \mu\text{m}$ ). Under load, many of these asperities deform elastoplastically. During sliding, tensile stresses can develop at the base of the asperities, particularly on the asperity's backside, leading to crack propagation or stress corrosion and subsequent wear. This mechanism is likely responsible for wear in artificial joints and in other cases where polymers slide on very smooth surfaces.

The wear process considered above is not the only possible wear mechanism but is expected to dominate unless the roughness of the counter surface is very small. In the latter case, significantly smaller wear rates are anticipated compared to those observed for the tile and sandpaper surfaces.

Another wear mechanism is adhesive wear. Adhesive wear is particularly important for metals [28]. In asperity contact regions, local pressures can break the oxide coating present on most metals, resulting in direct metal-to-metal contact. If the metals are of similar composition, such as steel against steel, cold-welded junctions may form, leading to material transfer between the sliding objects. This phenomenon has been confirmed in experiments using radioactive metals to trace material transfer.

The transferred material contains oxide film fragments, and the exposed free metal oxidizes, forming a transferred film enriched with oxides. This film binds to the base metal less strongly than the internal binding within the metals. Consequently, after sufficient sliding time, oxide-rich wear particles form. Initially, these particles may become trapped between the sliding surfaces, but eventually, they leave the interface as wear debris.

## 8 Summary and conclusion

We have presented experimental data for the wear rate of polymethyl methacrylate (PMMA) sliding on a tile surface, on sandpaper, and on a polished steel surface, and for silica glass and quartz sliding on sandpaper. The experimental results were compared to a recently developed theory of sliding wear [1]. We find generally good agreement between the theory and experiments, but two open problems remain:

(a) The theory predicts similar wear rates for window (soda-lime-silica) glass and quartz (crystalline  $\text{SiO}_2$ ), as they have very similar elastic moduli and penetration hardness. However, experimentally, the wear rate for quartz is approximately 0.16 times smaller than that for window glass. This discrepancy may be related to the fact that window glass is amorphous, while quartz is crystalline. Plasticity in crystals arises from the generation and motion of dislocations, whereas in amorphous solids, plasticity results from local rearrangements of the atoms in nanometer-sized domains. These differences could lead to variations in work-hardening and flow properties, which are not accounted for in our simple elastoplastic description of the solids.

(b) For PMMA on the tile surface, the theory predicts that a large number (on the order of a few hundred) of contacts with wear asperities are necessary to remove a single wear particle. Due to the relatively short sliding distance in the experiments, it is unclear whether this is the case. We have suggested (see Discussion section) that this may require a reinterpretation of the relationship between  $\gamma$  and  $\Delta x$  (the Paris curve), where the crack tip moves in a stochastic manner, exhibiting finite (and possibly rather large) displacements  $\Delta x$  in some asperity contacts, and no displacement in others.

**Acknowledgments:** We thank M. Ciavarella for useful discussions. This work was supported by the Strategic Priority Research Program of the Chinese Academy of Sciences, Grant No. XDB0470200.

**Author declarations:** The authors have no conflicts to disclose. All authors have contributed equally.

**Data availability:** The data that support the findings of this study are available within the article. The data that support the findings of this study is available from the corresponding author upon reasonable request.

**Appendix A** We have studied the ploughing tracks on a soda-lime glass block (a), a boro-silica glass block (b), and a quartz block (c) after they were slid a short distance on a sandpaper P100 surface (see Fig. 20). A detailed study showed that even for these brittle materials much of the material removed below the undeformed

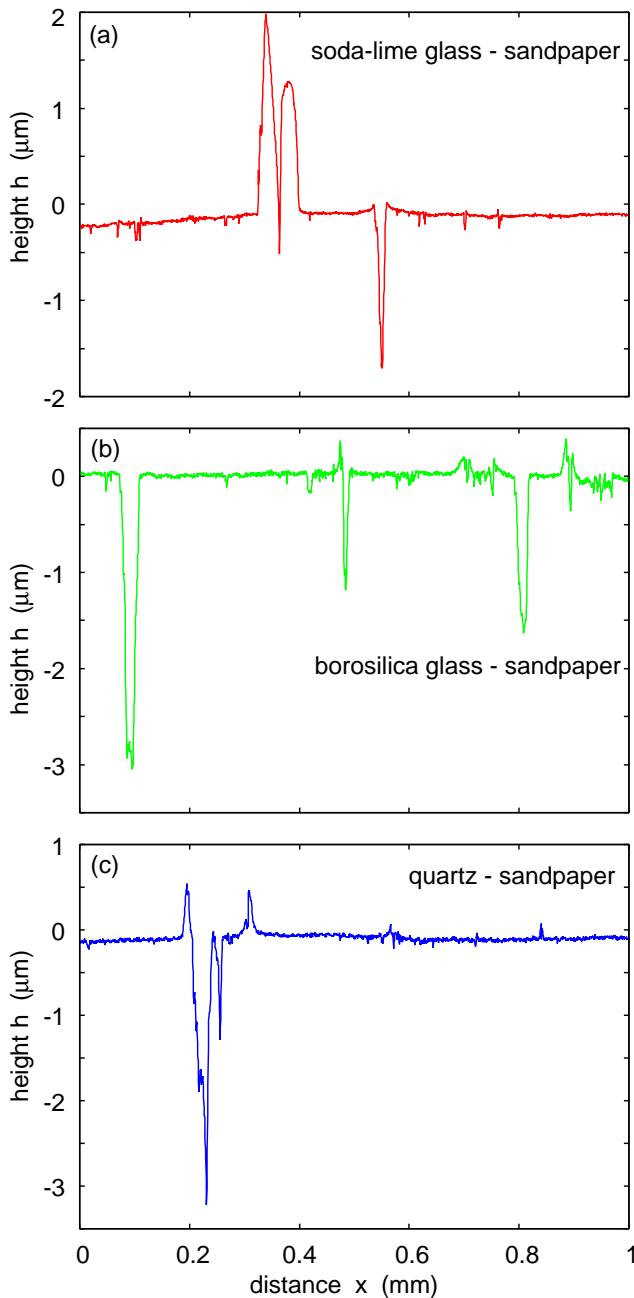


FIG. 20. The height profile orthogonal to the wear or ploughing tracks after a soda-lime glass block (a), boro-silica glass block (b), and a quartz block (c) was slid a short distance on a sandpaper P100 surface. An analysis of 25 mm long wear tracks showed that most of the glass removed from the wear tracks does not form wear particles but is plastically displaced on the surface.

surface plane was plastically displaced to above the undeformed surface plane. The width of the ploughing tracks are  $\sim 50 \mu\text{m}$  or less.

- [1] B. N. J. Persson, R. Xu, N. Miyashita, *Rubber wear: experiment and theory* Journal of Chemical Physics (accepted).
- [2] J.F. Archard, *Contact and rubbing of flat surfaces*, J. Appl. Phys. **24**, 981 (1953).
- [3] R. Holm, *Electric Contacts*, Almqvist and Wiksell, Stockholm (1946)
- [4] E. Rabinowicz, *The effect of size on the looseness of wear fragments*, Wear **2**, 4 (1958).
- [5] E. Rabinowicz *Influence of surface energy on friction and wear phenomena*, Journal of Applied Physics **32**, 1440 (1961).
- [6] R. Aghababaei, D.H. Warner and J.F. Molinari, *Critical length scale controls adhesive wear mechanisms*, Nature Communications **7**, 11816 (2016).
- [7] L. Frerot, R. Aghababaei and J.F. Molinari, *A mechanistic understanding of the wear coefficient: From single to multiple asperities contact*, Journal of the Mechanics and Physics of Solids **114**, 172 (2018).
- [8] J. Choudhry, A. Almqvist, R. Larsson, *Improving Archard's Wear Model: An Energy-Based Approach*, Tribology Letters **72**, 93 (2024).
- [9] S. Pham-Ba and J.-F. Molinari, *Adhesive Wear Regimes on Rough Surfaces and Interaction of Micro-contacts*, Tribology Letters **69**, 107 (2021).
- [10] R.S. Dwyer-Joyce, R.S. Sayles and E. Ioannides, *An investigation into the mechanisms of closed three-body abrasive wear*, Wear **175**, 133 (1994).
- [11] T.C. Buttery and J.F. Archard, *Grinding and abrasive wear*, PIQC. Inst. Mech. Eng. **185** 537 (1971).
- [12] Werner JH, Rosenberg JH, Keeley KL, Agrawal DK, *Immunobiology of periprosthetic inflammation and pain following ultra-high-molecular-weight-polyethylene wear debris in the lumbar spine* Expert Rev Clin Immunol. 2018;14(8):695-706. doi:10.1080/1744666X.2018.1511428
- [13] R. Stocck, *Some Revisions of Fatigue Crack Growth Characteristics of Rubber*, Adv Polym Sci [https://doi.org/10.1007/12\\_2020\\_72](https://doi.org/10.1007/12_2020_72)
- [14] A.N. Gent, *Adhesion and Strength of Viscoelastic Solids. Is There a Relationship between Adhesion and Bulk Properties?*, Langmuir **12**, 4492 (1996).
- [15] P. Ghosh, R. Stocck, M. Gehde, R. Mukhopadhyay and R. Krishnakumar, *Investigation of fatigue crack-growth characteristics of NR/BR blendbased tire tread compounds*, Int. J. Fract. **188**, 9 (2014).
- [16] R. Rivlin and A. Thomas, *Rupture of rubber. I. Characteristic energy for tearing*, J. Polymer Sci. **10**, 291 (1953).
- [17] J. Rong, J. Yang, Y. Huang, W. Luo and X. Hu, *Characteristic Tearing Energy and Fatigue Crack Propagation of Filled Natural Rubber*, Polymers **13**, 3891 (2021).
- [18] M.H. Müser and A. Wang, *Contact-Patch-Size Distribution and Limits of Self-Affinity in Contacts between Randomly Rough Surfaces*, Lubricants **6** 85 (2018).
- [19] B.N.J. Persson, *Theory of rubber friction and contact mechanics*, The Journal of Chemical Physics **115**, 3840 (2001).
- [20] T.G. Bifano, T.A. Dow and R.O. Scattergood, *Ductile-mode grinding: A new technology for machining brittle materials*, Journal of Engineering for Industry **113**, 184 (1991).
- [21] M.A. Davies, Y. Chou, and C.J. Evans, *On Chip Mor-*

- phology, *Tool Wear and Cutting Mechanics in Finish Hard Turning*, CIRP Annals **45**, 77 (1996).
- [22] E.K. Antwi, K. Liu and H. Wang, *A review on ductile mode cutting of brittle materials*, Front. Mech. Eng. **13**, 251 (2018).
- [23] U.D. Hangen, *Time-Dependent Deformation Behavior of PMMA*, Bruker Application Note # 1513  
[https://industronnano.com/wp-content/uploads/2020/09/Polymer-AN1513-Rev-A0\\_Time-Dependent-Deformation-Behavior-of-PMMA-\\_2018.pdf](https://industronnano.com/wp-content/uploads/2020/09/Polymer-AN1513-Rev-A0_Time-Dependent-Deformation-Behavior-of-PMMA-_2018.pdf)
- [24] W. Hong and Z. Xiulin, *The formulae of fatigue crack propagation in polymethyl methacrylate*,  
<https://www.gruppofrattura.it/ocs/index.php/ICF/ICF10/paper/viewFile/5013/7020>
- [25] E. Enriques, A. del Campo, J.J. Reinoso, G. Konstantopoulos, C. Charitidis, J.F. Fernandez, *Correlation between structure and mechanical properties in a-quartz single crystal by nanoindentation, AFM and confocal Raman microscopy* Journal of Materials Research and Technology **26**, 2655 (2023).
- [26] M. Barlet, J-M Delaye, T. Charpentier, M. Gennisson, D. Bonamy, T. Rouxel, and C.L. Rountree, *Hardness and toughness of sodium borosilicate glasses via Vickers's indentation*, Journal of Non-Crystalline Solids **417-418**, 66 (2015).
- [27] A. Dey, R. Chakraborty, and A.K. Mukhopadhyay, *Nanoindentation of Soda Lime-Silica Glass: Effect of Loading Rate*, International Journal of Applied Glass Science **2**, 144 (2011)
- [28] J.A. Greenwood, *Metal Transfer and Wear* Frontiers in Mechanical Engineering **6**, 1 (2020).



